

Green Chemistry

Accepted Manuscript



This is an *Accepted Manuscript*, which has been through the RSC Publishing peer review process and has been accepted for publication.

Accepted Manuscripts are published online shortly after acceptance, which is prior to technical editing, formatting and proof reading. This free service from RSC Publishing allows authors to make their results available to the community, in citable form, before publication of the edited article. This *Accepted Manuscript* will be replaced by the edited and formatted *Advance Article* as soon as this is available.

To cite this manuscript please use its permanent Digital Object Identifier (DOI®), which is identical for all formats of publication.

More information about *Accepted Manuscripts* can be found in the [Information for Authors](#).

Please note that technical editing may introduce minor changes to the text and/or graphics contained in the manuscript submitted by the author(s) which may alter content, and that the standard [Terms & Conditions](#) and the [ethical guidelines](#) that apply to the journal are still applicable. In no event shall the RSC be held responsible for any errors or omissions in these *Accepted Manuscript* manuscripts or any consequences arising from the use of any information contained in them.

Real-time monitoring of the deactivation of HZSM-5 during upgrading of pine pyrolysis vapors

Calvin Mukarakate¹, Xiaodong Zhang², Alexander R. Stanton³, David J. Robichaud¹, Peter N. Ciesielski⁴, Kara Malhotra⁵, Bryon S. Donohoe⁴, Erica Gjersing¹, Robert J. Evans⁶, David S. Heroux⁷, Ryan Richards⁸, Kristiina Iisa¹ and Mark R. Nimlos¹

¹National Bioenergy Center, National Renewable Energy Laboratory, 15013 Denver West Parkway, Golden, CO 80401-3393

²Energy Research Institute of Shandong, Academy of Sciences, Jinan 250014, China

³Department of Chemical and Biological Engineering, Colorado State University, Fort Collins, CO 80523

⁴Biosciences Center, National Renewable Energy Laboratory, 15013 Denver West Parkway, Golden, CO 80401-3393

⁵Department of Mechanical and Aerospace Engineering, Cornell University, Ithaca, NY 14853

⁶MicroChem Technologies Inc. 2983 Sterling Ct, Boulder, CO 80301

⁷Department of Chemistry, St. Michael's College, Colchester, VT 05439

⁸Department of Chemistry and Geochemistry, Colorado School of Mines, Golden, CO 80401

Abstract

The conversion of pine pyrolysis vapors over fixed beds of HZSM-5 catalyst was studied as a function of deactivation of the catalyst, presumably by coking. Small laboratory reactors were used in this study in which the products were identified using a molecular beam mass spectrometer (MBMS) and gas chromatography mass spectrometry (GCMS). In all of these experiments, real-time measurements of the products formed were conducted as the catalyst aged and deactivated during upgrading. The results from these experiments showed the following: 1) Fresh catalyst produced primarily aromatic hydrocarbons and olefins with no detectable oxygen-containing species. 2) After pyrolysis of roughly the same weight of biomass as weight of catalyst, oxygenated products begin to appear in the product stream. This suite of oxygen containing products appears different from the products formed when the catalyst is fresh and when the catalyst is completely deactivated. In particular, phenol and cresols are measured while upgrading pine, cellulose and lignin pyrolysis vapors, suggesting that these products are intermediates or side products formed during upgrading. 3) After the addition of more pyrolysis vapors, the product stream consists of primary vapors from pine pyrolysis. Catalysts samples collected at various points during deactivation were analyzed using a variety of tools. The results show that carbon build-up is correlated with catalyst deactivation, suggesting that deactivation is due to coking. Further, studies of nitrogen adsorption on the used catalyst suggest that coking initially occurs on the outside of the catalyst, leaving the micropores largely intact. From a practical point of view, it appears that based upon this study and others in the literature, the amount of oxygen in the pyrolysis products can be related to the level of deactivation of the HZSM-5 catalyst, which can be determined by how much pyrolysis vapor is run over the catalyst.

Corresponding author

E-mail: calvin.mukarakate@nrel.gov

1. INTRODUCTION

There has been a recent surge of interest in converting biomass into liquid transportation fuels because of the potential for reduced carbon emissions versus fossil fuels, the desire for increased national energy security, and the support for local economic development. The production of hydrocarbon fuels using fast pyrolysis is particularly attractive as it produces up to 75 wt% carbonaceous oil, called bio-oil,¹ which with upgrading could be used as a fuel blending material or a feedstock for further processing. Bio-oil contains oxygen functional groups (aldehydes, ketones, phenolics, acids, etc), which are derived from the oxygen in plant biopolymers and contribute to undesirable properties such as high acidity, high viscosity, low heating value, immiscibility with hydrocarbons and instability.¹⁻⁶ Wood typically has an elemental composition⁷ of about 50 wt% carbon, 6 wt% hydrogen and 44 wt% oxygen or an atomic composition of $C_1H_{1.4}O_{0.7}$ and bio-oil from fast pyrolysis⁴⁻⁶ contains approximately 53 wt% carbon, 6 wt% hydrogen and 41 wt% oxygen. Thus, the oxygen content remains essentially unchanged, but the material is converted to an unstable liquid. Hydrotreating^{8, 9} is one approach actively being developed to improve the stability and remove the oxygen from raw pyrolysis oil. Another promising approach is to catalytically upgrade the pyrolysis vapors before they are condensed, which is called catalytic fast pyrolysis (CFP).

Though other catalysts have been used, zeolites and especially HZSM-5 have been favored for upgrading biomass pyrolysis vapors.^{9, 36} These catalysts are effective for the conversion of methanol to gasoline (MTG)³⁷⁻⁴¹ and early studies with biomass pyrolysis vapor⁴² produced aromatic hydrocarbons with high octane ratings (> 100) and favorable properties for blending with gasoline. More recent studies^{17, 34} produced similar results, but suffered from low yields (10 – 15 wt% of biomass). The low yields were a result of high gas production (30 – 40 wt% of biomass) and coke build up on the catalyst (10 – 20 wt% of biomass). Since biomass is typically expensive (50 – 100 \$/ton),⁴³ low product yields represent a significant technical barrier towards the development of this technology. In addition, the coke build up on the catalyst, rapidly deactivates it. For MTG the coking rates are much lower (< 1 wt%).³⁷⁻⁴¹ The difference in coking rates for methanol and biomass pyrolysis vapors can be understood in terms of the effective hydrogen index (EHI), which is the hydrogen to carbon ratio after oxygen has been removed as water, $EHI = (H/C)_{eff} = (H - 2*O)/C$, where H, O and C are the atom compositions. For methanol, the EHI is 2.0, which is the ideal stoichiometry for the production of olefins (C_nH_{2n}). Conversely, biomass pyrolysis vapor has an EHI of approximately 0.2, a stoichiometry that is more favorable to forming coke.

In order to better understand coking and yields from upgrading pyrolysis vapors with HZSM-5, several parametric studies have been conducted where reaction conditions have been varied. Temperatures from 400 °C to 650 °C have been investigated and it was found that coking rates can be decreased with increasing temperature, but this results in greater cracking and the formation of more light gases (CO, CO₂, light hydrocarbons).³⁴ A number of studies also varied the exposure level of the catalyst to the biomass vapors. These experiments were conducted using fixed or fluidized bed reactors and products were measured after a fixed exposure of the catalyst to the pyrolysis vapors. Here we have compiled the results of these experiments in an effort to understand what they tell us about deactivation and yields. Of the numerous studies of catalytic upgrading, several were selected for this analysis because they used

HZSM-5 at an operating temperature of about 500 °C, with varying exposure levels.^{12, 17, 25, 28, 34, 35} Interestingly, these studies report varying yields and oxygen levels in the resulting oils, but they can all be related based upon the deactivation of the catalyst, presumably due to coke build-up. Deactivation is likely due to the exposure of the catalyst to the pyrolysis vapor and one can plot the amount of oxygen in the oil and the liquid yield as functions of the biomass-to-catalyst ratio as is shown in Fig. 1. This data appears to follow a monotonic function that increases asymptotically to values obtained when biomass is pyrolyzed in the absence of a catalyst. We have fit the oxygen data to an exponential function to provide clarity. This suggests that catalyst that is fresh initially produces very low yields of essentially oxygen-free hydrocarbons, but as the amount of biomass is increased, the catalyst becomes deactivated and oxygenated products breakthrough, increasing the yield and oxygen content of the oil. From this plot it appears that for biomass-to-catalyst ratios greater than 3 or 4, the catalyst appears to be completely deactivated.

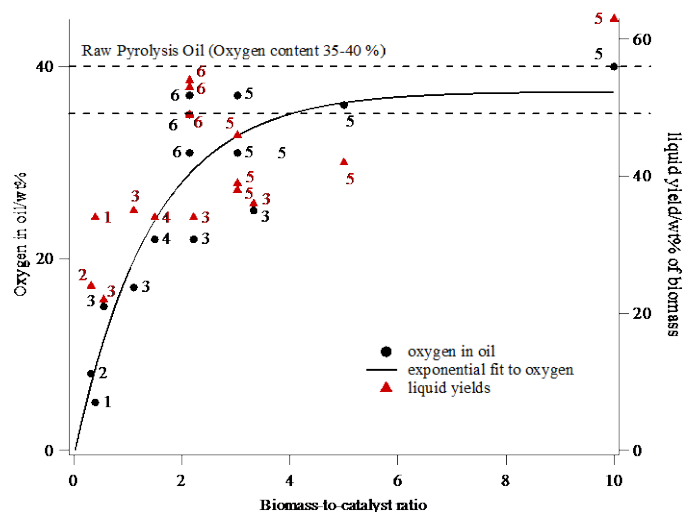


Fig. 1. Literature results for oxygen content in the bio-oil for CFP using HZSM-5 vs. biomass-to-catalyst ratio. The line is an exponential fit to the oxygen data. Number in the plot correspond to the following reference: 1 is ref¹⁷, 2 is ref³⁴, 3 is ref²⁵, 4 is ref¹², 5 is ref³⁵, and 6 is ref²⁸.

The question we address here is whether this observed variation in oxygen content can be explained by partial deactivation of the catalyst caused by coke formation. Coke causes catalyst deactivation by occluding pores or poisoning active sites. In order to minimize the amount of oxygen in the CFP bio-oil, we need to understand the reaction mechanisms that form coke, and also characterize its properties. Detailed reaction mechanisms for formation of both desirable and undesirable products during CFP of biomass using HZSM-5 remain elusive, even though some mechanisms have been proposed.^{10, 11, 32, 33, 44} These studies proposed that biomass primary vapors are upgraded to hydrocarbons and olefins by HZSM-5 through a series of reactions comprising cracking, deoxygenation, oligomerization, cyclization, aromatization, isomerization and polymerization. Coke is formed from polymerization of aromatic hydrocarbons and/or condensation of unreacted lignin primary vapors.⁴⁴ The mechanism for coke formation in HZSM-5 during methanol-to-olefin (MTO) conversion has been reported.³⁹ This study proposed that aromatics or alkenes present in the zeolite pores and/or its intersections form a “hydrocarbon pool” (HP) responsible for formation of light olefins and aromatics. The same species in the HP

can also add to the initial aromatic products to form larger, polyaromatic compounds and ultimately coke, which deactivates the catalyst.

Characterization of coke formed during biomass CFP can lead to a better understanding of the mechanisms involved in its formation. Coke characterization on zeolites has been extensively studied for petroleum reactions and several reviews of coke characterization have been published.⁴⁵⁻⁴⁷ One study discussed the chemistry of coke formation, emphasizing the importance of hydrogen transfer, condensation, and rearrangement steps at high temperatures.⁴⁷ There have been few studies of coke characterization from upgrading of biomass-based streams. One report analyzed properties of coke formed on several different types of zeolites during catalytic pyrolysis of pine,⁴⁸ and another report characterized the coke formed from catalytic cracking of pyrolysis oil over HZSM-5.⁴⁹ Since biomass vapors already contain a low amount of hydrogen, any dehydration reactions occurring within the zeolite pores will further reduce the hydrogen content in the vapor. If we apply the above MTO hydrocarbon pool idea to biomass CFP, the pool resulting from the deoxygenation of biomass pyrolysis vapors will be deficient in hydrogen, which will favor molecular weight growth reactions, eventually forming larger aromatic molecules (coke). This coke can quickly block acidic sites within the HZSM-5 pores, thereby reducing the activity and lifetime of the catalyst,^{16, 34} but more importantly it directly leads to the increase of oxygen concentration in the resulting bio-oil as shown in Fig. 1.

In this study we examine upgrading of pyrolysis vapors over HZSM-5 during deactivation in order to determine if the pyrolysis vapors are simply breaking through the catalyst or if reaction intermediates are being formed. An understanding of the deactivation process and coke build-up will allow the optimization of biomass-to-catalyst ratio and the development of processes to reduce coke formation. We monitored in real-time the change in product distribution of the upgraded vapors as a function of HZSM-5 catalyst deactivation using a molecular beam mass spectrometer (MBMS). Product identification was confirmed using py-GCMS. Coked catalyst samples were collected at various points during deactivation and they were characterized using several analytical tools including thermogravimetric analysis (TGA), ¹³C NMR, N₂ physisorption, Raman spectroscopy, atomic force microscopy (AFM), and energy dispersive spectroscopy (EDS).

2. EXPERIMENTAL METHODS

We conducted experiments to measure the CFP products through mass spectrometry, and the properties of coke formed on the catalyst. Initial studies were conducted with a horizontal reactor connected to a molecular beam mass spectrometer and a pyroprobe-GCMS with a separate vertical catalyst bed to rapidly screen and determine changes in product stream as the catalyst deactivates. The horizontal reactor was used for rapidly measuring products from CFP of cellulose, lignin, and pine. The pyroprobe was used for confirming the identity of the CFP products. In both reactors, pulses of biomass were pyrolyzed and passed over a fixed bed of catalyst. Additional experiments were conducted using a microreactor, where pine was continuously fed. Samples of catalyst were collected at different stages of deactivation and were analyzed to understand the coking process.

Avicel cellulose was bought from Sigma Aldrich. Sulfur-free straw lignin from Asian Lignin Manufacturing (ALM) obtained from non-woody plants (grass) was supplied by Granit SA, Lausanne, Switzerland. Southern yellow pine was supplied by Idaho National Laboratory (INL). Typically, southern yellow pine contains approximately 42 % cellulose, 21 % hemicellulose, and 30 % lignin. The carbon, hydrogen, and nitrogen contents of these feedstocks were measured using a LECO TruSpec CHN module, and the oxygen content was measured by difference.^{21, 50} Table 1 shows the elemental composition of the feedstocks. A proprietary HZSM-5 catalyst was supplied by Albemarle. The structure of a standard MFI catalyst can be found on <http://www.iza-structure.org/databases/>. In these studies we used a regenerated catalyst. The catalyst had undergone approximately ten catalytic pyrolysis and regeneration cycles in a two-inch bubbling fluidized bed reactor.¹⁷ CFP in those experiments was performed at 500-550°C and regeneration was achieved by burning at 650°C in a nitrogen-air mixture until no CO or CO₂ was detected in the effluent gas. The activities of the fresh catalyst and the regenerated catalyst for aromatic hydrocarbon formation were the same within experimental uncertainty as determined in the Pyroprobe-GCMS system (vide infra). Experiments with both pine and catalyst in the pyrolysis zone in the ratio of 10:1 at 600°C gave aromatic hydrocarbon yields of 20±5% and 21±2% for the fresh and regenerated catalyst, respectively.

Table 1. Elemental composition of biomass materials.

Feedstock	Ultimate Analysis (wt. %)			
	C	H	N	O
Cellulose	44.3	6.2	<0.01	49.5
Lignin	62.7	6.0	1.1	28.6
Pine	41.6	6.9	0.08	50.6

2.1 Horizontal Reactor-MBMS

This reactor system was used for initial pulsed experiments to study the deactivation process of HZSM-5. It consisted of a horizontal quartz annular flow tube reactor coupled with an MBMS.²¹ Batch-wise pyrolysis and vapor upgrading took place in the inner tube where the vapors were carried in a 0.2 slm flow of helium. The flow in the inner tube was mixed with a 4 slm helium flow from the outer tube at the end of the reactor, before it was sampled by the MBMS orifice. Diluting with the outer flow helps reduce secondary reactions and helped meet the flow demands of the sampling orifice. Quartz boats containing 50 mg samples of biomass were introduced into the 500 °C flow in the inner tube. Approximately 50 boats were consecutively pyrolyzed during a typical experiment using a fixed bed of 1.0 g HZSM-5 catalyst. On average, each pulse of vapors from pyrolysis of 50 mg pine lasted for 30 s, implying an instantaneous space hourly velocity of approximately 3.6 hr⁻¹. The reactor was heated to the desired temperature using a five-zone furnace. The vapors for each pulse were then sampled by the MBMS orifice.

The MBMS^{19-21, 51, 52} has been extensively used for on-line, real-time sampling of the products of the pyrolysis of biomass. The sampled gases undergo adiabatic expansion through a 250 μm orifice into a vacuum chamber held at ~100 mtorr. This expansion cools the gas and effectively freezes the chemistry. The cooled gas is skimmed into a molecular beam, and is then ionized with an electron impact ionization source (22.5 eV), producing positive ions that are measured using a quadrupole mass spectrometer. In these experiments, a mass spectrum with an m/z range of 10-500 was

collected every second. The MBMS can measure signals for a wide variety of molecular species from the pyrolysis of biomass and the upgrading of the vapors. In the CFP experiments, a small, precisely controlled flow of argon (40 sccm) mixed with helium carrier gas was used as a tracer gas to correct for drifts in the signal due to change in flow through the molecular beam inlet. This allowed us to compare relative concentrations among experimental conditions, even though the concentrations were not quantified.

2.2 Pyroprobe-GCMS

A pyroprobe analytical pyrolyzer (model 5200HP-R, CDS Analytical Inc.) coupled to a GCMS was used in conjunction with the horizontal reactor-MBMS experiments. This system consists of two computer controlled resistively heated elements, one for pyrolyzing pine samples (pyrolysis zone) and another one for catalytic upgrading of the pyrolysis vapors (upgrading zone). A trap filled with Tenax-TA™ (a polymer resin poly (2, 6 diphenyl-p-phenylene oxide) was placed after the upgrading zone to adsorb the upgraded vapors. To monitor deactivation of HZSM-5, several 1 mg pine samples were pyrolyzed consecutively and the vapors were upgraded using a fixed bed of 10 mg catalyst until the total biomass-to-catalyst ratio was 2. During experiments, products from the pyrolysis zone entrained in He carrier gas flowed through the upgrading zone and then through the trap. Most of light gases passed through the trap, but vapors were adsorbed onto it. After 3 minutes, the flow was switched so that the He carrier gas was passed through the trap into an Agilent G1530A gas chromatograph (GC) interfaced with a HP 5973 mass spectrometer (MS). The trap was heated to 400 °C to desorb the adsorbed vapors. However, the transfer lines from the trap to the GC can only be heated up to a maximum of 325 °C, meaning that the high molecular weight condensable products such as lignin dimers or three ring aromatic hydrocarbons (boiling points > 325 °C) can condense on these lines. The CFP interface was held at 70 °C and the GC injector was operated at 275 °C. A constant He flow of 52 ml min⁻¹ was maintained in the capillary column (Agilent 190915-433) equipped with a stationary phase consisting of 5 % phenyl and 95 % dimethyl polysiloxane. This column was used to separate the condensable vapors from the CFP process. The GC oven was programmed with the following temperatures: hold at 40 °C for 3 min then heated up to 240 °C with 6.0 °C min⁻¹. The separated CFP species were identified using the NIST GCMS library. The residence time of the pyrolysis vapors was estimated to be about 0.03 s and the mass hourly velocity 21 h⁻¹ based on pyrolysis vapors.

2.3 Microreactor-MBMS

This reactor system was used for continuous feeding of biomass into a reactor with a fixed bed of HZSM-5 catalyst. It consists of a quartz microreactor system equipped with a computer controlled continuous feeder, as depicted in Fig. 2. The feed unit consisted of a hopper, dual auger, and two inlets for He carrier gas. The hopper holds up to 10 g of milled biomass, but only 5.0 g of pine were used in each experiment. The pine wood particles (1-2 mm) from the hopper were fed into the reactor by a dual Delrin® auger system. Prior to feeding pine, the hopper was purged with He introduced through one of the inlets at a flow rate of 400 sccm to remove air in the feeding unit. Helium introduced in the second inlet was used for entraining the pyrolysis vapors. The microreactor was housed in a tube furnace with five zones independently controlled and heated to 500 °C before beginning the experiment. Pyrolysis occurred at the top of the reactor and was separated from the catalytic vapor phase upgrading step by ceramic frits. In addition to entraining pyrolysis vapors, He gas was

used as a sweeping gas to quench secondary reactions by dilution. The flow rate of the transporting He was 400 sccm and that of the diluent He was 3500 sccm.

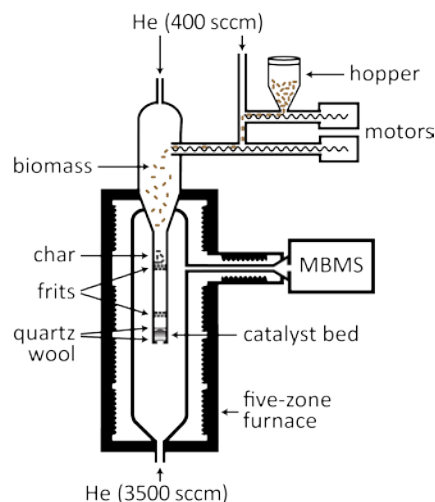


Fig. 2. Microreactor-MBMS system for studying vapor phase upgrading of biomass pyrolysis. The figure shows a dual auger continuous feeder, closely coupled pyrolysis and catalytic upgrading zones and an MBMS.

The experiments were carried out with the reactor interfaced directly to the MBMS for on-line product analysis. The diluent He carried the upgraded vapors into the source of the mass spectrometer with minimal condensation or additional thermal cracking on the hot reactor surfaces. All catalytic upgrading experiments were conducted using approximately 1.0 g of catalyst or replacing the catalyst with sand for non-catalytic runs. The catalyst was loaded into the reactor tube (I.D. =7.5 mm) resulting in a catalyst bed volume of approximately 1.0 cc. At a carrier gas flow rate of approximately 400 sccm, the residence time of the pyrolysis vapors in the catalyst bed was approximately 0.4 seconds at 500 °C. Typically, an experimental run consisted of continuously feeding pine onto a quartz frit in the pyrolysis zone. Pine was fed at a rate of approximately 7 g/hr. Thus, 5.0 g of pine were fed over approximately 45 minutes. In these experiments, the mass hourly velocity based on pyrolysis vapors (60% of biomass mass) was approximately 4 hr⁻¹.

2.4 Multivariate Analysis of MBMS Spectra

Multivariate analysis was used to identify groups of mass spectral peaks that were correlated in the product vapors and to track their trends as the catalyst deactivated. We used the multivariate curve resolution optimized by alternating least squares (MCR-ALS) routine available in the statistical analysis software package The Unscrambler (Camo Software AS, version 9.7). Multivariate Curve Resolution (MCR) resolves the principal component analysis results into mathematically constructed components which have mathematically derived sub-spectra that are used to partition the original variance of the data set into estimates of the concentrations of the components.⁵³ This allows the determination of elution profiles of the components in an unresolved mixture of two or more constituents, assuming the data has enough degrees of freedom to identify the separate sources of variance. This is useful since mixtures experienced in this experimental work are not available as pure components. The Unscrambler MCR algorithm is based on pure-variable selection from PCA loadings to find the initial estimation of spectral profiles, and

then Alternative Least Squares (ALS) to optimize resolved spectral and concentration profiles. We included the constraints for producing non-negative concentration profiles and non-negative mass spectra. We did not apply constraints for unimodality and equality in concentration profiles so that the variation of relative concentrations for pure components (PCs) with biomass-to-catalyst ratio represented the data accurately. Further details on the application of multivariate analysis on biomass pyrolysis and gasification can be found elsewhere.^{19, 52, 53}

2.5 Coke Characterization

Coke deposited on the catalyst was analyzed by thermogravimetric analysis (TGA), ¹³C NMR, N₂ physisorption, Raman spectroscopy, atomic force microscopy (AFM), and energy dispersive spectroscopy (EDS). For the thermogravimetric determination a TGA Instruments Q500 analyzer was used. The samples were heated in air at 10 and 20 °C/min to a final temperature of 900 °C. For NMR, cross polarization magic angle spinning (CPMAS) NMR spectra were collected on a Bruker Avance 600 spectrometer equipped with a 3.2 mm CPMAS probe and a 14.1 T magnet (¹H = 600.16 MHz and ¹³C = 150.9 MHz). A ramped CP pulse with ¹H and ¹³C fields matched at 55 kHz was applied with a contact pulse of 1 ms. An acquisition time of 0.0226 s and a recycle delay of 5 s were used with 2,000 points collected and averaged over 15,000 scans for each spectrum with MAS = 22 kHz. Resonance Raman spectra were collected from catalyst particles at various points of deactivation using a Horiba Jobin Yvon LabRam spectrometer with a 244 nm excitation laser at a power of 15 mW.

AFM imaging was used to characterize the topography and changes in the overall surface roughness of the catalysis using a Nanoscope V Multimode scanning probe microscope from Bruker. The catalyst particles were mounted on an SPM magnetic sample mounting disk. A TESP-SSW tip was used for the surface characterization with a drive frequency of the cantilever around 320 kHz, a spring constant of 42 N/m and a nominal tip radius of 2 nm. Scanning sizes were 500 nm x 500 nm with a scan rate of 0.46 Hz. The data were flattened by planar background subtraction using Nanoscope Analysis software (Bruker). Surface roughness was calculated from 3 sub-regions of interest from each image also using the aforementioned software. Catalyst particles were imaged and analyzed by energy dispersive X-ray spectroscopy (EDS) using a FEI Quanta 400 FEG instrument equipped with an EDAX X-ray detector. Samples were mounted on aluminum stubs with conductive carbon tape adhesive and sputter-coated with 7 nm of irridium prior to imaging; uncoated samples were used for EDS analys. Elemental composition was obtained from the EDS spectra using the EDAX Genesis software package.

2.6 N₂ Physisorption

N₂ physisorption at 77K from P/P₀ 0.01 to 1 was conducted on a Micromeritics TriStar II. Samples were degassed under He flow prior to analysis. During the experiments they were heated to 90 °C for one hour before heating at 350 °C for 8 hours. Adsorption-desorption isotherms were collected and the surface area was calculated by the BET method. Pore volume was calculated by the BJH method. High resolution micropore analysis was conducted on a Micromeritics ASAP 2020 equipped with low pressure transducers. Samples were degassed under vacuum at 350 °C for 8 hours prior to analysis and were then transferred to the analysis port and adsorbed volume and free space was experimentally determined. They were subsequently re-degassed on the analysis port at 350 °C for 4 hours before being

measured by incremental dosing in order to collect 50 data points below P/P₀ of .01. Micropore size was determined by the Horvath-Kawazoe method with Saito-Foley correction for cylindrical pores.⁵⁴

3. RESULTS AND DISCUSSION

3.1 Product distribution as a function of catalyst deactivation

3.1.1 Horizontal Reactor-MBMS

Fig. 3 shows mass spectra averaged over the 500 °C pyrolysis of three 50 mg samples of cellulose (lower), lignin (middle) and pine (upper). Pyrolysis of 50 mg of cellulose took 35 s, lignin took 26 s and pine took 33 s, and their corresponding average char yields were 3.5 %, 36 % and 12 % respectively. The duration of the pyrolysis vapors and char yields are comparable to previous batch pyrolysis studies.^{19, 21} The spectra in Fig. 3 consist of oxygenated hydrocarbons including aldehydes, ketones, alcohols, carboxylic acids and phenolics in addition to H₂O, CO and CO₂.^{19, 20, 30, 55} Pine is a softwood, which means that the lignin components of pine pyrolysis vapors contain only one methoxy group on the phenolic ring (i.e. G subunits). Thus, lignin primary vapors predominantly consist of 2-methoxyphenol derivatives; guaiacol (2-methoxyphenol) *m/z* 124, methyl guaiacol *m/z* 138, 4-vinyl guaiacol *m/z* 150, vanillin *m/z* 152, isoeugenol *m/z* 164, and the heaviest monomer peak, *m/z* 180 which represents coniferyl alcohol. The sugar components of pine pyrolysis vapors are represented by furan ring derivatives; furan *m/z* 68, furfuryl alcohol *m/z* 98 and 5-hydroxymethyl furfural or levoglucosone *m/z* 126, and 1,4:3,6-dianhydro- α -D-glucopyranose *m/z* 144, and low molecular weight products; acetic acid and glycoaldehyde *m/z* 60. The peaks at *m/z* 43, 55, 57, and 73 are known carbohydrate fragment peaks.^{19, 52} The sugar component of pine vapors match up very well with the spectrum of pyrolysis of cellulose shown in the lower panel of Fig. 3. However, the lignin sample used in this study was extracted from grass, which means that the lignin vapors will consist of H, G and S subunits.⁵⁶ Additional peaks observed from pyrolysis of this lignin sample include, vinyl phenol *m/z* 120, syringol *m/z* 154, and 4-vinyl syringol *m/z* 168.

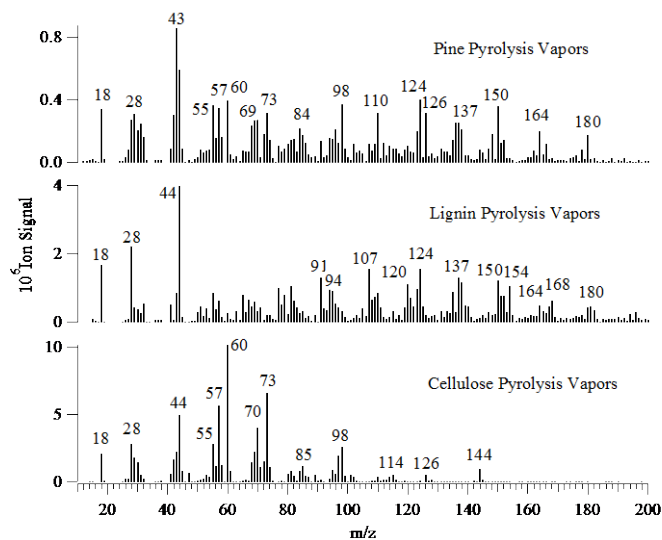


Fig. 3. Mass spectra for 500 °C pyrolysis products from 50 mg each of cellulose (lower panel), lignin (middle panel), and pine (upper panel) recorded using the horizontal reactor-MBMS system.

During the CFP experiments, approximately 50 boats, each containing 50 mg of biomass, were pyrolyzed one at a time and the vapors were passed over a fixed bed of 1.0 g HZSM-5 catalyst. Fig. 4A shows total mass spectral ion counts of three boats recorded at different points of the experiment. The ion count profile for boat 1 was recorded after vapors from pyrolysis of the first 50 mg of pine were passed through the catalyst bed. The ion count profiles for boat 12 and boat 47 were recorded after pyrolysis of a total of 0.6 g and 2.35 g of pine respectively. Fig. 4B shows the corresponding averaged mass spectra recorded for boat 1, 12 and 47. Without considering the shoulders, the duration for the pulses from boats 1, 12, and 47 are 28 s, 30 s and 33 s respectively. The differences in pulse intensities are due to the activity of the catalyst. Notice from the mass spectra that the intensities of the peaks are comparable for all the boats, but there are fewer peaks in the spectra from boat 1, because the catalyst is active and only olefins and aromatic compounds are formed. As the catalyst deactivates, more products are formed and the total ion current increases as the pyrolysis vapors breakthrough the catalyst bed and more complex spectra are measured. The shoulders observed for ion profiles from boat 12 and boat 47 are due to desorption of coke precursors and intermediate species from the catalyst pores and surface by steam m/z 18 from the pyrolysis process. Note that the shoulder is not present on the ion profile from boat 1. The averaged mass spectrum collected for boat 1 is dominated by olefins and aromatic hydrocarbons; propylene m/z 42, butene m/z 56, benzene m/z 78, toluene m/z 92, xylene m/z 106, indene m/z 116, trimethyl benzene m/z 120, naphthalene m/z 128, methyl naphthalene m/z 142 and dimethyl naphthalene m/z 156 and oxygen in the primary vapors is rejected as H_2O , CO and CO_2 . Note that most compounds present in the pine primary vapors were deoxygenated to form olefins and aromatic hydrocarbons irrespective of their functional groups.

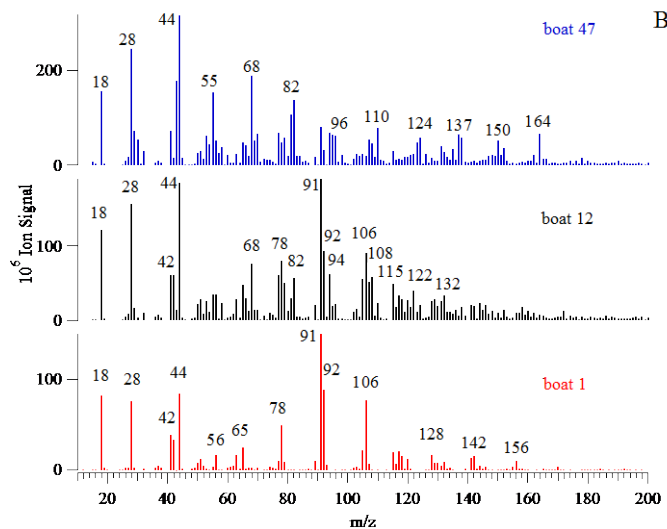
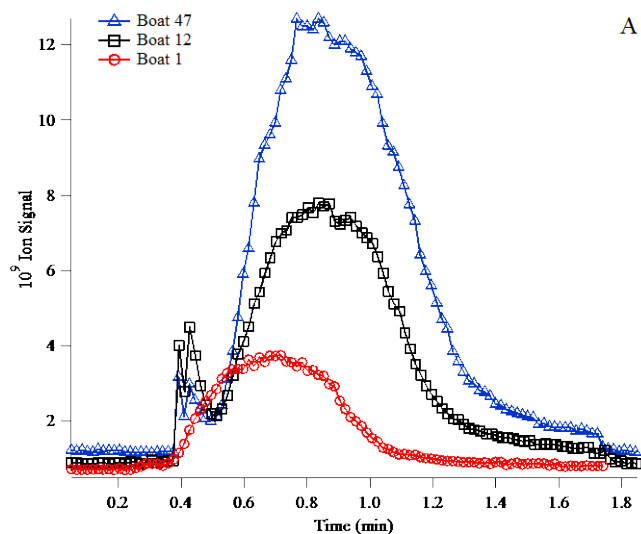


Fig. 4. Example data for CFP of 50 mg of pine per boat recorded using the horizontal reactor-MBMS system. A) Total ion count profiles for pulses of pyrolysis vapor run over catalyst at different points (boat 1, boat 12 and boat 47) of the experiment. B) Corresponding averaged mass spectra recorded for these pulses.

The pore sizes of HZSM-5 catalysts are approximately 5 Å,⁵⁷ and therefore heavy primary vapors with sizes larger than 5 Å, which cannot enter the pores would need to undergo catalytic cracking on the macrosurface to form light species.^{10, 11, 32, 33} The produced light species will be deoxygenated and then oligomerized to form olefins. Some light species and olefins will escape from the micropores. Olefins retained in the micropores will undergo further oligomerization, alkylation and isomerization reactions to form aromatic hydrocarbons.^{10, 11, 32, 33} Running in parallel to these reactions are polymerization and condensation reactions that result in formation of the undesirable coke. Condensation reactions occur during formation of coke from primary vapors, and polymerization reactions occur during formation of coke from aromatic hydrocarbons.⁴⁴

When coke is formed, it deactivates the catalyst by blocking pores, which contain active sites. The spectrum in the upper panel of Fig. 4B was collected after the 47th boat was introduced for a total of 2.35 g of biomass. At this point the catalyst was largely deactivated because this spectrum is similar to that measured for the raw pyrolysis vapors from pine shown in Fig. 3. It contains lignin pyrolysis products seen in raw pine pyrolysis vapors (m/z 110, 124, 137, 138, 150, 152 and 164), while some of the furans peaks (m/z 68, 82, and 96) are enhanced. This suggests that the catalyst was deactivated for the conversion of lignin pyrolysis products, but still partially active for the conversion of carbohydrate products. The spectrum in the middle panel, after 12 boats, contains a suite of products with a different spectral pattern. It has several peaks observed from the spectra of boat 1 and boat 47, plus some additional new peaks. These new peaks can be assigned to phenol m/z 94, cresol m/z 108, methyl cresol m/z 122 and methyl benzofuran m/z 132, and we believe that these arise from intermediate species formed during the CFP of pine vapors. This result implies that the composition of the product stream changes with the amount of coke deposited on the catalyst, or that these intermediates are initially held up by the catalyst. Since they are more polar than the non-oxygenated

aromatics detected for boat 1, they are likely to be more tightly bound in the catalyst.

The mass spectrum for boat 12 in Fig. 4B shows that the activity of HZSM-5 does not change instantaneously from being fully active to complete deactivation. It shows strong overlapping of CFP products, thus analysis of this data set requires a multivariate approach. In order to identify product trends occurring during deactivation of the catalyst resulting from the sequential pyrolysis of 48 boats of pine, we used the multivariate curve resolution-alternating least squares (MCR-ALS) routine. We prepared a data set with dimensions (48 boats x 130 masses). The top 130 masses with the largest variances were selected for this analysis. The goal for MCR is to mathematically decompose our data set of overlapping mass spectra into pure contribution of each component involved during CFP of the 48 boats. In this case MCR-ALS analysis was optimized for three pure components (PCs), which gave real molecular peaks with largest resolutions, excluding modeling of noise in the data set. Increasing the PCs beyond three did not cause a significant reduction in the residual error. The loadings for these three PCs are shown in Fig. 5A. As can be seen PC 1 is roughly the same as the mass spectrum obtained when the first boat of pine was introduced into the reactor. This is the mass spectrum obtained when pine pyrolysis vapors were passed over fully active catalyst, producing water, CO, CO₂, olefins and aromatic compounds. PC 3 is roughly the same as the spectrum that was obtained after introduction of boat 47 after which the catalyst was deactivated for the lignin pyrolysis products but partially active for the carbohydrate products. Thus, this PC contains peaks for lignin primary pyrolysis products, some carbohydrate primary products and intense furan peaks.

The multivariate analysis has extracted a pure component, PC 2, which has a distinct set of mass spectral peaks, punctuated with peaks for furans, phenol and cresols (furan m/z 68, methyl furan m/z 82, dimethyl furan m/z 96, phenol m/z 94, cresol m/z 108, methyl cresol m/z 122, methyl benzofuran m/z 132). We believe that some of these mass spectral features arise from reactive intermediates or side products that are formed during catalytic reaction of the pyrolysis vapors with the catalyst. Thus, PC 1 contains primarily deoxygenated organic species, olefins and aromatic compounds, PC 2 contains some oxygenated intermediates and PC 3 contains the oxygenated molecules similar to primary pyrolysis vapor. The plot for the scores of the three PCs as a function of biomass-to-catalyst ratio, Fig. 5B, shows the trend of these groups of molecules during deactivation. At the start of the experiment, only the olefins and aromatic molecules (PC 1) are present. Note that the signal for this component increases over the first five boats of pine, up to a biomass-to-catalyst ratio of 0.2. This could be the induction period that is often observed during methanol-to-olefin processes³⁹ and is a result of the buildup of hydrocarbon species inside the catalyst pores or intersections. After the products build up to a critical point, they are released into the gas phase. The same reaction mechanisms that form aromatic hydrocarbons could also lead to polymerization reactions that form coke. This could block some active sites in the catalyst, which could lead to the observed onset of the formation of the species in PC 2 at a biomass-to-catalyst ratio of 0.2. However, the observation of these species may not be an indication of deactivation, but simply desorption due to high buildup of these intermediates in the catalyst. The intermediate species in PC 2 (furans, phenol and cresols) reach a maximum at approximately 0.8.

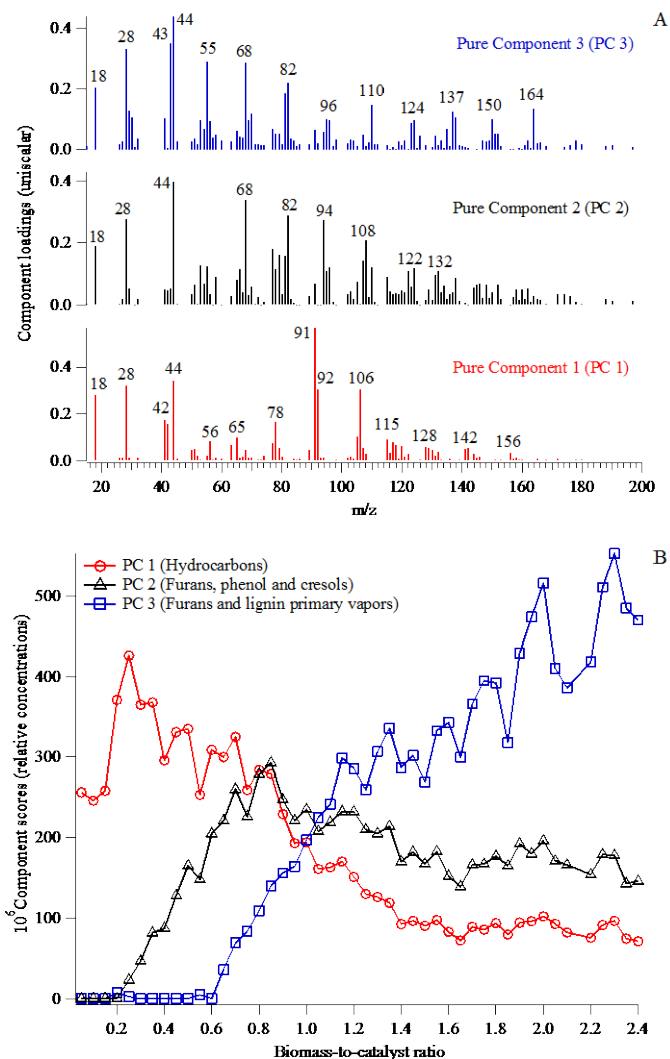


Fig. 5. A. The reconstructed spectra for each pure component (PC 1 to PC 3) from MCR-ALS analysis of CFP of 48 boats of pine over 1.0 g HZSM-5 in the horizontal reactor, revealing changes in the composition of the product stream as the catalyst deactivates. Note, the reconstructed spectra are unit-vector normalized. B. The component scores from MCR-ALS analysis of CFP experiment show the dependency of each PC with biomass-to-catalyst ratio. The loadings spectra are shown in Fig. 5A.

It should be noted some mass variables appear in both PC 2 and PC 3 including furans, phenol, and cresols. The advantage of using the multivariate approach over a univariate representation of the trends is that the correlation-based MCR is the basis of a lumped portrayal of the changes that can overcome some of the limitations of the low resolution mass spectra. This means that compounds which may persist beyond the maxima of PC 2 are still represented in the suite of products associated with the intermediate chemistry. Mass variables with more than one contributing compound can be partitioned between the two groups. For example, m/z 124 can be due to methyl catechol, a PC 2 compound, and methoxyphenol, which would likely be best classified as PC 3. The use of a single compound to represent the trend would mask this distinction.

As the run time of the catalytic upgrading process increases, polymerization reactions of the aromatic hydrocarbons start to form large aromatic species that can plug the catalyst micropores. This further deactivates the catalyst up to a point where some primary vapors (e.g. methoxyphenols) break through the catalyst bed beginning at a biomass-to-catalyst ratio of 0.6. At the same time the intensities of deoxygenated hydrocarbons start to decrease because the catalyst is losing activity. The species in PC 3 (furans and lignin primary vapors) then appear in the mass spectra and increase until the end of the experiment. The formation of these products is a clear indication that the catalyst is starting to deactivate, as these products are similar to the starting materials. We will show that there is coke formation on the external surface (mesopores) of the catalyst. This likely arises from condensation reactions of unconverted lignin primary products and polymerization of aromatic hydrocarbons. These reactions continue until all the micropores are capped with coke, deactivating the catalyst.

To further explore the formation of the intermediate species (PC 2), we repeated the above experiment using cellulose and lignin biopolymers. The goal was to determine if species in PC 2 were either intermediates of CFP or primary pyrolysis vapors breaking through the catalyst. As Fig. 3 shows, furans and phenols are present in the primary vapors of pine pyrolysis. These species have also been measured in condensed pyrolysis oils.⁵⁵ Thus, it is possible that these feed molecules breakthrough earlier than the rest of compounds in the primary vapors. As Fig. 3 shows, the primary vapors from cellulose do not contain phenolic compounds, and their observation during the upgrading over HZSM-5 would suggest that these molecules are intermediates or side products. As with pine upgrading, 50 boats containing 50 mg of cellulose were inserted into the horizontal reactor, and we used MCR-ALS to analyze the (50 x 130) data set. The MCR-ALS analysis for this data set was also optimized for three pure components, because increasing PCs beyond three did not result in significant change of the residual error. PC 1 consisted of hydrocarbon products, similar to those from upgrading pine pyrolysis vapors (olefins and aromatics). PC 2 consisted of furan derivatives (furan, methyl furan, dimethyl furan and trimethyl furan) and interestingly, phenol and cresol. The observation of phenol and cresol supports our hypothesis that these are intermediates or side products formed during upgrading. The mass spectrum of PC 3 is similar to the spectrum for pyrolysis of cellulose shown in Fig. 3 implying that PC 3 signals deactivation of the catalyst. The loadings spectra for cellulose are provided in the supplementary materials (Fig. S1). The pure component scores for cellulose as a function of biomass-to-catalyst ratio are plotted in the lower panel of Fig. 6. As with pine, only PC 1, olefins and aromatic compounds, is observed initially, with a short induction period. At a biomass-to-catalyst ratio of approximately 0.1, PC-2 is observed and gradually increases until a maximum at a ratio of 1.6. PC3 again starts to break through at 0.6 and continues to grow throughout the experiment. These results also show that deactivation of cellulose occurs at approximately the same biomass-to-catalyst ratio as for pine. Perhaps this is not surprising, since carbohydrates make up 63 % of pine and pyrolysis of the carbohydrates produces more primary vapors and less coke than lignin.

For lignin, 34 boats containing 50 mg of lignin were inserted into the horizontal reactor, and we used MCR-ALS to analyze the (34 x 130) data set. The MCR-ALS analysis for this data set was also optimized for three pure components; PC 1 consisted of the same hydrocarbons as pine and cellulose. However, PC 2 consisted of phenol, cresol, methyl cresol, dimethyl cresol and cyclopentadiene

m/z 66. It is important to note that PC 2 did not have any furan derivatives. PC 3 consisted of the lignin primary vapors shown in Fig. 3. The loadings spectra for lignin are provided in the supplementary materials (Fig. S2). The upper panel of Fig. 6 shows the scores of these three PCs for lignin as a function of biomass-to-catalyst ratio. PC 1 dominates at biomass-to-catalyst ratios below 0.2, shows a small induction period and then decreases throughout the experiment. For cellulose there is gradual increase of both PC 2 and PC 3 compared to sharp increases for lignin starting at ratios of 0.2 and 0.4. The intermediate species, PC-2, reaches a maximum at a ratio of 0.5 compared to 1.8 for cellulose. This suggests more rapid deactivation for the lignin pyrolysis products, due to higher rates of coking. This is even more striking when one considers the vapor yields from lignin compared to cellulose. Cellulose experiments produced 4 wt% char, meaning that at least 96 wt% of the 50 mg was passed over HZSM-5, whereas lignin produced 36 wt% char, meaning that approximately 64 wt% of the 50 mg was passed over the catalyst.

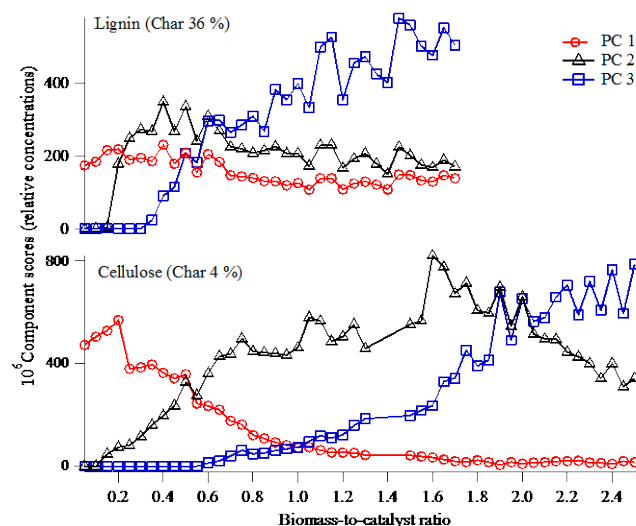


Fig. 6. The component scores from MCR-ALS analysis of CFP of biopolymers using 1.0 g HZSM-5 in the horizontal reactor. The lower panel shows results from CFP of 50 boats of cellulose. The upper panel shows results from CFP of 34 boats of lignin. The loadings spectra are shown in supplementary figures (S1 and S2).

This study reveals that the composition of the product stream changes with increase in biomass-to-catalyst ratio, which is proportional to the amount of coke deposited on the catalyst. There appear to be three points where the change in composition of the product stream is clearly noticeable; 1) when the spectrum contains hydrocarbons (olefins and aromatics) only, 2) when the intermediates are formed, 3) when the primary vapors begin to breakthrough. The intermediates observed in 2) appear to be primarily phenols and cresols.

3.1.2 Pyroprobe-GCMS

To identify products and complement the MBMS analysis, similar pulsed experiments using py-GCMS were carried out. In these experiments, the fixed-bed contained 10.0 mg of HZSM-5 and 1.0 mg samples of pine were pyrolyzed until the biomass-to-catalyst ratio was 2. Both pyrolysis and catalysis temperatures were maintained at 500 °C. As mentioned in the experimental section, the light gases were not detected in our mass spectrometer and high molecular weight condensables were condensed on transfer lines. This limited

the range of species that were detected by the GCMS. Fig. 7 shows three chromatograms for vapors that were desorbed from the trap.

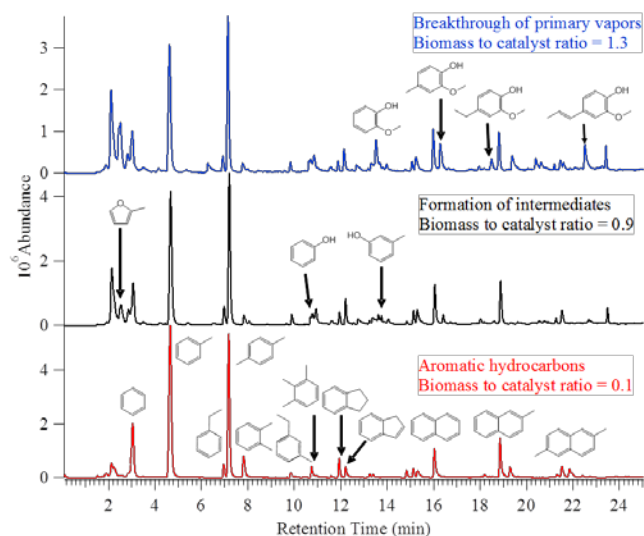


Fig. 7. Chromatograms from CFP of 1.0 mg of pine over 10 mg HZSM-5 at different points of the experiment showing changes in the composition of the product streams as the catalyst deactivates.

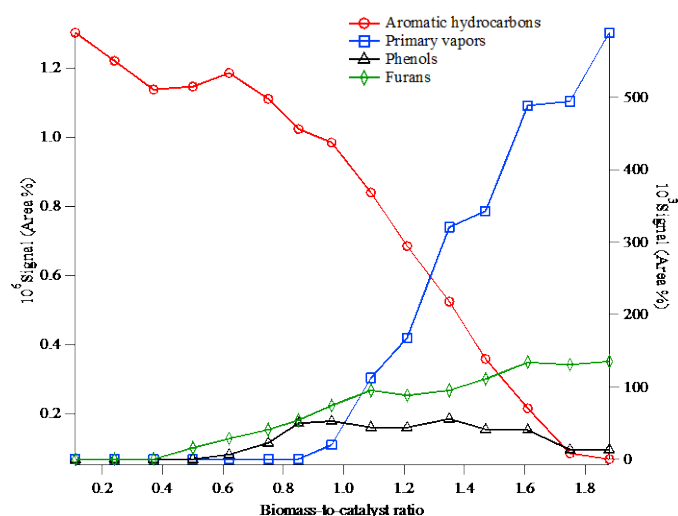


Fig. 8. Variation of py-GCMS product classes with deactivation of HZSM-5 catalyst. The aromatic hydrocarbons (left axis only) include benzene, toluene, ethyl benzene, p-xylene, o-xylene, styrene, indene, indane, trimethyl benzene, ethyl toluene, methyl indene, naphthalene, methyl naphthalene and dimethyl naphthalene, the phenols include phenol, o-cresol, m-cresol and p-cresol, the furans include methyl furan and methyl benzofuran and the primary vapors include acetic acid, furfural, 2-methoxyphenol, 4-methyl-2-methoxyphenol, 4-vinyl-2-methoxyphenol, 4-ethyl-2-methoxyphenol, 3-propenyl-2-methoxyphenol, 4-propenyl-2-methoxyphenol and 4-propyl-2-methoxyphenol.

The lower panel was recorded when the biomass-to-catalyst ratio was 0.1. This chromatogram shows only aromatic hydrocarbons and

no oxygenated species were found in the vapors. It is dominated by one- and two-ring aromatic compounds (C_6 - C_{14}); benzene, toluene, ethyl benzene, p-xylene, o-xylene, 1-ethyl toluene, 1,2,3-trimethyl benzene, indane, indene, naphthalene, 2-methyl naphthalene and 2,6-dimethyl naphthalene.^{17, 20, 21, 44} The middle panel was recorded when the cumulative biomass-to-catalyst ratio was 0.6. This chromatogram now contains oxygenated species methyl furan, phenol and m-cresol in addition to the dominant aromatic hydrocarbons. The upper panel was recorded when the cumulative biomass-to-catalyst ratio was 1.3. This chromatogram contains furans, phenol, cresols and lignin primary vapors (2-methoxyphenol, 4-methyl guaiacol, etc.).⁵⁵ Table 2 lists the compounds observed from the py-GCMS study, including the biomass-to-catalyst ratios at which each species first appeared in the chromatogram.

The py-GCMS results agree very well with the py-MBMS study, in that there are three distinct points (biomass-to-catalyst ratios) where the composition of the product stream changed. These points are depicted in Fig. 8, which shows the variation of the composition of the product stream with biomass-to-catalyst ratio. As with the MBMS, only aromatic compounds were observed initially. At a biomass-to-catalyst ratio of 0.4, the intermediates were formed and gradually increased. The phenols were formed when this ratio was 0.5. Phenol and cresol increased and then leveled off before they decreased to zero. At a ratio of 0.8 the lignin primary vapors started to breakthrough and continued to grow sharply throughout the experiment. At this point the majority of carbohydrates pyrolysis products were still being upgraded to furans. Fig. 8 shows that the composition of the product stream changes as the catalyst bed is apparently deactivated. The py-GCMS also allowed us to identify additional peaks which were not observed during the MBMS study, such as cyclohexadiene, cyclopentenones, furfural and acids. Fig. S3 in the supplementary shows a modified Fig. 8, which includes the variation of these additional species with biomass-to-catalyst ratio. Cyclohexadiene started to breakthrough at a biomass to catalyst ratio of 0.5, gradually increased to reach a maximum at a ratio of 1, and disappeared from the chromatograms at a ratio of 1.5. Cyclohexadiene profile was similar to that of the intermediates (furans, phenol and cresols) meaning that it might belong to this group. Cyclopentenones started to breakthrough at a ratio of 1 and gradually increased throughout the experiment. At high biomass-to-catalyst ratios (> 1.6) the product stream was composed of mostly lignin primary vapors. At these ratios some sugar pyrolysis products, such as furfural and acetic acids started to breakthrough and gradually increased throughout the experiment. We also observed phenol and cresol during CFP of cellulose and lignin using the py-GCMS. The results are shown in the supplementary Fig. S4. The mechanism for formation of phenol and cresol from CFP of cellulose is still elusive, considering the complex nature of biomass vapor compared to the MTG. To the best of our knowledge there is no published work on formation of phenol and cresol during the MTG process, however phenol has been observed during conversion of furan on HZSM-5⁵⁸ and also during self-condensation reactions of acetone on HZSM-5 catalyst.⁵⁹⁻⁶¹ The acetone studies discuss mechanisms for formation of phenolics on HZSM-5. Acetone is a biomass pyrolysis product¹⁹ and its reaction mechanism on HZSM-5 might shed light into how these phenolics are formed from CFP of cellulose.

3.1.3 Microreactor-MBMS

We used this reactor to conduct continuous feeding of pine pyrolysis vapors over the HZSM-5, as opposed to the pulsed experiments above. Continuous feeding is a more realistic option for commercial

scale CFP systems. 5.0 g of pine were fed at a rate of 7 g hr⁻¹ and the pyrolysis vapors were passed over a fixed bed of 1.0 g HZSM-5 catalyst. Pyrolysis and catalytic upgrading sections of the reactor were held at 500 °C. Initial tests were performed using sand in place of HZSM-5 and we observed the same products for pine primary vapors as shown in Fig. 3 and reported in literature.^{19, 20, 30, 55} Tests conducted using a fully active HZSM-5 produced a mass spectrum dominated by olefins and aromatic hydrocarbons ranging from one- to two- ring aromatics as discussed in the above pulsed studies. To get a clear picture of how the composition of the product stream changed with continuous feeding of pine, the data from the microreactor-MBMS study was also subjected to MCR-ALS analysis. As with the pulsed experiments, the MCR-ALS analysis was optimized for three pure components. PC 1 consisted of aromatic hydrocarbons; one-ring (benzene *m/z* 78, toluene *m/z* 92 and xylenes *m/z* 106), two-ring (naphthalene *m/z* 128, methyl naphthalene *m/z* 142 and dimethyl naphthalene *m/z* 156), and three-ring (phenanthrene *m/z* 178 and methyl phenanthrene *m/z* 192). PC 2 consisted of phenol and cresols (phenol *m/z* 94, cresol *m/z* 108, methyl cresol *m/z* 122, naphthol *m/z* 144, and methyl naphthol *m/z* 158). Additional species at *m/z* 65, 77 and 91 were also observed in this PC. Note that no furans were observed in this PC, which is different to the pulsed experiments above. This is likely a result of more complete deactivation in this experiment. Thus, the furans are included in the component with the primary vapors. The mass spectrum of PC 3 contained the furans and lignin pyrolysis vapors. The loadings spectra for CFP of pine in the microreactor showing these results are provided in the supplementary materials (Fig. S5). The pure components scores for pine as a function of biomass-to-catalyst ratio are plotted in Fig. 9. As with the py-MBMS and py-GCMS studies above, at low biomass-to-catalyst ratios, only PC 1 (deoxygenated hydrocarbons) is observed, it increased sharply to reach a maximum at a ratio of approximately 0.5, stays constant until a ratio of 1.3, and then decreased gradually to zero at a ratio of 2.7. At a biomass-to-catalyst ratio of approximately 0.8, PC 2 is observed and gradually increases until a maximum at a ratio of 1.6, and then decrease and level off at a ratio of 3.0. PC 3 starts to break through at 1.5 and levels off at a biomass-to-catalyst ratio of about 3, which is roughly where apparent complete deactivation occurred in the literature studies shown in Fig. 1.

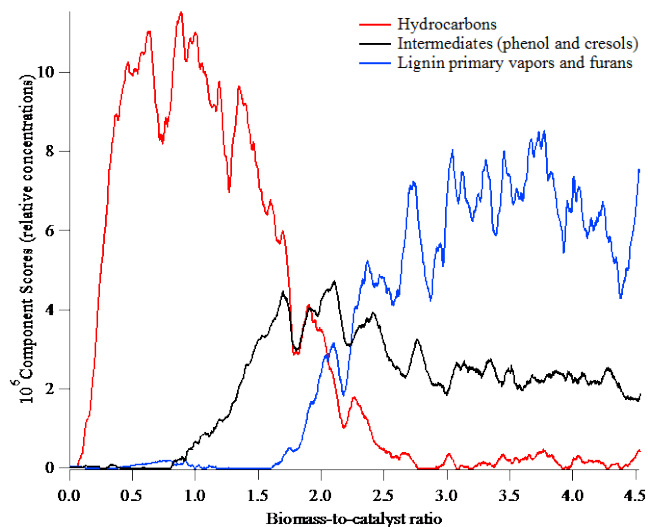


Fig. 9. The component scores from MCR-ALS analysis of CFP of 5.0 g of pine over 1.0 g HZSM-5 using the microreactor-MBMS system

showing the dependency of each PC with biomass-to-catalyst ratio. The loadings spectra are shown in Fig. S5.

3.2 Catalyst Analysis

To further investigate deactivation mechanisms, we collected four HZSM-5 samples from various points during deactivation using the microreactor-MBMS system. Continuous feed experiments, such as that shown in Fig. 9, were conducted and the feed was stopped at various points as determined by monitoring the MBMS signal. Sample 1 was collected by stopping the feed at a biomass-to-catalyst ratio of 0.4. At this point the catalyst appeared to be fully active because there was no formation of intermediates or breakthrough of primary vapors. Sample 2 was collected at a ratio of 1.0, after the intermediates (phenol and cresols) were formed. We collected sample 3 at a ratio of 1.7, after the primary vapors (methoxyphenols) began breaking through the catalyst. Sample 4 was collected after we finished feeding all 5 g of pine. Each catalyst sample was thoroughly mixed and then analyzed using several analytical techniques including, ¹³C NMR, Raman spectroscopy, EDS, AFM, N₂ physisorption and TGA.

The HZSM-5 deactivation was caused by carbonaceous deposits as evidenced by the black color of the catalyst (Figure S6). We performed experiments using ¹³C NMR and Raman spectroscopy to identify the molecular nature of these deposits. The results of the ¹³C NMR analysis are shown in Fig. 10. This spectrum agrees very well with previous ¹³C NMR coke characterization studies.⁶² It shows two distinct types of carbon: aromatic (120-150 ppm) and aliphatic (15-30 ppm). The aliphatic carbon, may be due to methyl groups linked to aromatics (peak at 19 ppm) and CH₂ groups linked to methyl groups (20-25 ppm).^{62, 63} No C-O bonds could be detected. The signals at 129 ppm and 19 ppm increase with increases in biomass-to-catalyst ratio because more carbonaceous deposits were formed with more time on stream. The signal-to-noise ratios are low due to the low coke content in the samples, and because of this, no quantification of the relative amounts of the aromatic and aliphatic carbons were made.

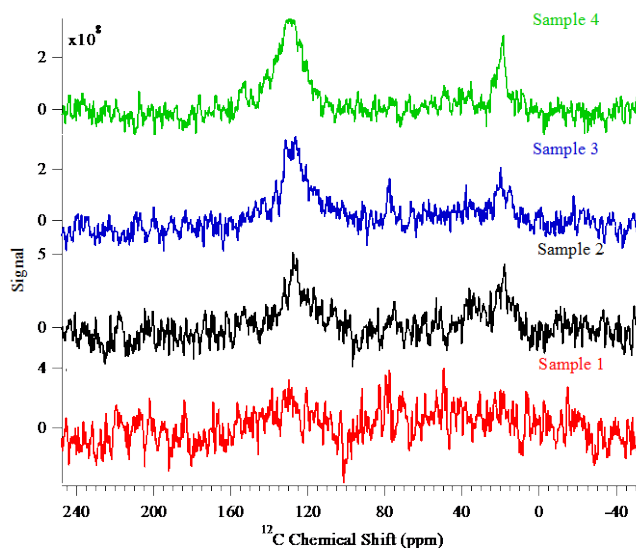


Fig. 10. ¹³C NMR analysis for coked catalyst samples obtained from the microreactor experiment. Sample 1 was collected at a biomass-to-catalyst ratio of 0.4. Sample 2 was collected at a ratio of 1.0. Sample 3 was collected at a ratio of 1.7. Sample 4 was collected at a ratio of 5.

The nature of the carbonaceous deposits was further investigated by Resonance Raman spectroscopy. During this experiment, a 244 nm excitation beam uniquely suited for characterization of aromatic compounds was used, because it is resonant with the electronic transitions of aromatic molecules, and it greatly enhances the probability of Raman scattering from these types of bonds. Spectra were collected from catalyst particles from each of the four samples as well as from a regenerated catalyst. Raman scattering at $1605\text{--}1615\text{ cm}^{-1}$ is attributed to ring stretching of polyaromatic compounds (Fig. 11). The regenerated catalyst exhibited the lowest intensity in the 1600 cm^{-1} region, and a trend of increasing intensity with biomass-to-catalyst ratio was observed. The scattering at $1360\text{--}1410\text{ cm}^{-1}$ is also attributed to ring stretches of polyaromatic species and is indicative of the deposition of these materials on the catalyst surface.^{62, 64, 65} No aliphatic C-H stretches were observed in the spectra ($200\text{--}3000\text{ cm}^{-1}$), suggesting that the aliphatic peaks observed in the NMR were not due to aromatic methyl groups. The observation of aromatic peaks in the NMR and the Raman spectra suggest that coke is being formed in the catalyst and that this is the likely mechanism of deactivation. Observation of the CH_2 groups in the NMR spectra but not in the Raman spectra suggests that aliphatic compounds are present.

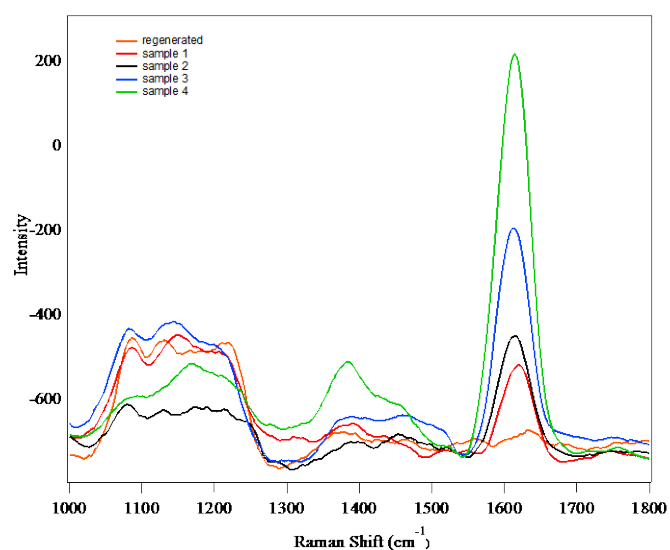


Fig. 11. Resonance Raman spectra of catalyst samples obtained from the microreactor experiment. The trend of increasing intensity in the 1600 cm^{-1} region is consistent with deposition of aromatic carbonaceous species on the catalyst samples as deactivation progresses.

Further characterization of the deposits on the catalyst samples was done using EDS and AFM. The EDS analysis was performed to probe elemental composition of the material deposited on the surface of the catalyst. Spectra were collected from multiple particles for each sample to quantify the variability of the elemental composition across the sample sets. The surface carbon content results are shown in Table 3. The surface carbon contents observed for sample 3 and sample 4 were significantly higher than that observed in the regenerated catalyst as well as catalyst particles for sample 2. The experimental error for the carbon content was larger than that of the other elements because the samples were mounted on carbon adhesive for analysis, thus contributions of this mounting medium

affected the EDS spectra near particle edges. EDS was also performed in a mapping mode to investigate the homogeneity of the film (Fig. 12A). The EDS maps show a general increase in surface carbon content that is largely uniform across the surface of the particles. The nanoscale surface geometry and roughness of catalyst particles for each sample was investigated by atomic force microscopy (AFM) (Fig. 12B). Table 3 shows that the surface roughness decreases with biomass-to-catalyst ratio, with sample 4 displaying significantly less nanoscale surface roughness than regenerated catalyst. These observations, in combination with the increased surface carbon content observed by EDS suggest the loss of structural definition at the scale of macroporosity is due to the deposition of a semi-continuous, carbonaceous film. This film contributes to the deactivation of the catalyst by blocking access to the pores of the catalyst particles and active sites therein.

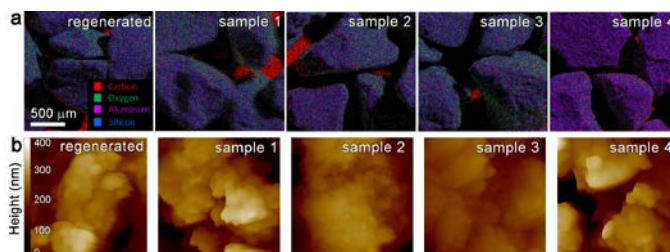


Fig. 12. a) EDS mapping provides a general view of macro-scale catalyst particle geometry and shows a trend of increasing carbon content on the particle surfaces with increase in biomass-to-catalyst ratio. b) Nanoscale surface topography was investigated by AFM. A trend of decreasing surface roughness was observed which is consistent with deposition of a bulk carbon film that decreases the definition of surface topography at later stages of deactivation.

The EDS and AFM would suggest that the deactivation of HZSM-5 was caused by coke capping the micropores. To investigate if any coke was formed inside the micropores, the four samples were analyzed using N_2 physisorption. Table 3 also lists a summary of textural properties from the N_2 physisorption study. The results are represented as percent reduction with respect to a regenerated HZSM-5 catalyst. The corresponding adsorption-desorption isotherms are shown in Fig. 13. The N_2 isotherms for all samples exhibit Type IV hysteresis indicating the presence of mesopores in addition to the micropores. The isotherms also exhibit a sharp increase in adsorption above $P/P_0 = 0.9$; from condensation between individual catalyst particles. The isotherms for samples 1 and 2 are very similar with the latter having slightly lower adsorption at all pressures. The decrease in the slope of both the adsorption and desorption in the mesopore region of these samples compared to the regenerated catalyst indicates that there is a decrease in pore size uniformity. These two samples also have approximately the same surface areas and pore volumes (Table 3). N_2 isotherms for samples, 3 and 4 show significant differences from the others. The isotherms exhibit a decrease in the quantity adsorbed and sample 3 has a 44 % surface area reduction compared to the regenerated catalyst. Sample 4 has a 67 % surface area reduction compared to the regenerated catalyst. Two features of the isotherms for sample 3 and sample 4 indicate that much of the coke formation occurs on the surface. The hysteresis for these samples remains open until ~ 0.45 where there is a fairly steep slope to close the hysteresis. This is most likely caused by the

formation of ink-bottle shaped pores during coke formation.⁶⁶⁻⁷¹ This can be explained by the partial capping of the pores by the coke on the surface allowing for N₂ pore filling at higher pressures but preventing desorption until P/P₀ of 0.45 typically found for ink-bottle pores.⁶⁶⁻⁷¹ The incomplete closing of the hysteresis below 0.4 also indicates that the pores are being capped as opposed to filled. The degree of separation between the adsorption and desorption lines are greater in sample 4 than sample 3. The most likely cause of the open hysteresis is N₂ filling in nearly completely capped pores at high pressures. At low pressures the gas is not able to escape easily and the rate at which the gas desorbs is much slower than allowed by the instrument to collect a stable pressure.

High resolution micropore analysis (Fig. 14) shows a significant decrease in the microporosity of the sample with biomass-to-catalyst ratio. Larger pores result in ink-bottle shaped pores, however micropores would be expected to be completely capped and unavailable for filling by N₂.⁷⁰ Fig. 14 shows that there is no significant difference between sample 1 and sample 2. This is supported by the roughly similar micropore volume reductions reported in Table 3. We believe that the observation of phenol and cresols is not due to catalyst coking because there is no significant changes in micropore volumes between sample 1 and sample 2. Sample 1 was collected when the catalyst was fully active and sample 2 was collected when we saw formation of phenol and cresols. This suggests that there is no significant deactivation of the catalyst due to plugging. Further as discussed above, there is some suggestion that phenols can be formed from upgrading of biomass model compounds. However, as with overall surface area sample 3 has about half the micropore volume as the regenerated catalyst and sample 4 has only 15% of the starting micropore volume indicating that nearly the entire surface for sample 4 is coated with coke. Table 3 also shows that the % reduction in pore volumes for samples, 1, 2 and 3, is roughly the same as that for the micropore volumes. However, the % reduction in micropore volume is much larger compared to % reductions for the pores for sample 4. This can be attributed to the coke formed in the mesopores capping the micropores in sample 4.

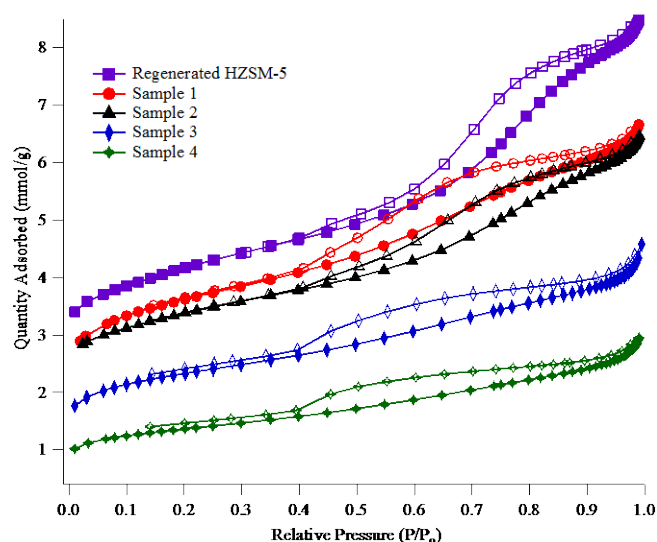


Fig. 13. N₂ Physisorption isotherms (77K) for; regenerated HZSM-5 catalyst and samples 1, 2, 3, and 4 obtained from the microreactor experiment.

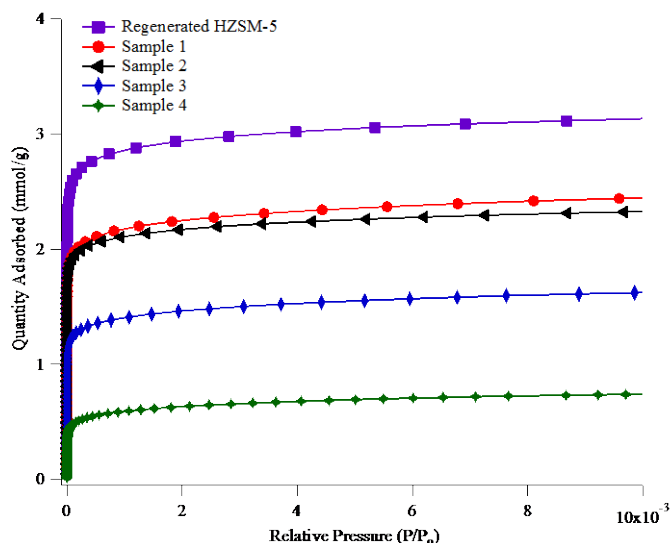


Fig. 14. High resolution, low pressure N₂ adsorption isotherms of the catalyst samples.

Since the N₂ physisorption results showed reductions in both the mesopore and micropore volumes, TGA was used to measure the amount of carbon built up on the catalyst. The goal was to distinguish between coke formed inside the micropores and coke formed on the mesopores. In the TGA, the samples were oxidized to measure the total amounts of coke on the catalyst, which are shown in Table 3. The amount of coke on catalyst originally increased relatively linearly with the biomass-to-catalyst ratio until the lignin primary vapors began breaking through (sample 3). Initially, 5-7% of the biomass was converted to coke until this breakthrough point. However, when proceeding from sample 3 to sample 4, the rate of coke formation decreased, and the fraction of biomass converted to coke during this interval decreased to 2.5%. Fig. 15 depicts a mass loss curve for combustion of sample 4. The mass loss below 250 °C was attributed to moisture and weakly adsorbed organic species in accordance with literature findings.^{45, 62} Rapid release of water below 175 °C is reported for zeolites with coke oxidation beginning at temperatures around 250 °C. Other studies reported coke evolution starting at 350 °C during upgrading of pyrolysis oil over HZSM-5.^{23, 45} Additional evidence for the mass loss below 250 °C being water was provided by the derivative curve generated from running a regenerated catalyst sample. The remaining mass loss from 250 °C to 700 °C was attributed to total coke.

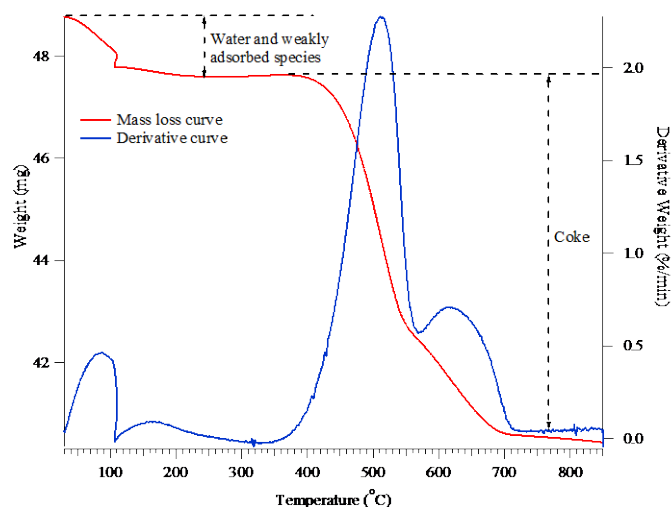


Fig. 15. Effect of temperature on combustion of coke deposited on catalyst sample 4.

The derivative curve in Fig. 15 indicates two regions for coke combustion: the main region with the highest rate of coke combustion around 500-525°C and a tail of more refractory coke around 575-675°C. Two or more regions of coke combustion are often reported.⁴⁵ The temperatures required to oxidize coke depend on the conditions at which coke is formed, location of the coke, and the zeolite type. Hydrogen-rich coke, so called type I coke or soft coke burns at low temperatures and highly polyaromatic coke, type II coke or hard coke, burns at higher temperatures starting around 425°C. Time on stream reduces the hydrogen contents of coke and shifts the oxidation to higher temperatures. Coke on ZSM-5 oxidizes at higher temperatures than coke on zeolites with larger pore sizes. The high oxidation temperatures in our samples are consistent with polyaromatic coke. The two regions might be due to coke on surface and between the zeolite crystals (mesopores) and coke in the zeolite micropores.^{23, 45} The aliphatic carbon observed in the ¹²C NMR data may be due to carbonaceous compounds in the micropores. During TGA experiments, the coke on the surface may be oxidized initially and then carbonaceous compounds containing aliphatic carbons will escape from the micropores. The fraction of the more refractory coke slightly decreased with time on stream. Sample 4 shows that approximately 70 % of the coke was in the main fraction (mesopores) and only about 30 % was in the more refractory coke fraction (coke in the micropores) whereas sample 1 shows 60 % coke in the mesopores and 40 % in the micropores. Our results suggest that the majority of coke was formed from polymerization and condensation reactions on the surface of the catalyst (mesopores).

4. CONCLUSIONS

This study has followed the evolution of products during the upgrading of biomass pyrolysis vapors over a fixed catalyst bed. Gas phase molecules were directly measured as pyrolysis vapors were continuously added, which showed changes as the catalyst, HZSM-5, evolved from being highly active to being completely deactivated. Along with measurements of the vapor phase products, we also characterized the catalyst to help understand the process of deactivation. The following list summarizes important findings from this work:

1. Complete deactivation of the catalyst with regard to the upgrading of pine pyrolysis vapor appears to occur at a biomass-to-catalyst ratio of about 3 as shown in Fig. 9. This is consistent with literature results using similar reaction conditions as shown in Fig. 1. Experiments with cellulose and lignin show that lignin pyrolysis vapors deactivate the catalyst quicker, while deactivation for cellulose vapors is about the same as for pine.
2. Between the stages of being active and completely deactivate, a suite of products containing phenols, cresols and methyl substituted phenols are observed. These products are observed with pine, lignin and cellulose and thus are not due to breakthrough of primary pyrolysis vapors. They are likely formed as intermediates or side products during catalytic upgrading. Their delayed observation may be due to partial deactivation or an induction period where sufficient build-up of these compounds is required before they are desorbed from the catalysts. Since they contain polar groups it is likely that they are held more tightly in the catalyst than the nonpolar aromatic compounds, such as toluene, which are desorbed earlier.
3. The measurement of these intermediates has not been reported in the literature and their observation may provide clues about the reaction mechanisms for hydrocarbon production. It is reasonable to expect that parts of that mechanism are similar to what has been proposed for the conversion of methanol in the methanol-to-olefin (MTO) or methanol-to-gasoline (MTG) processes. The reaction of methanol over fresh HZSM-5 catalyst produces similar products as is observed for cellulose, lignin and pine pyrolysis vapors. Thus, one can assume that the generalized hydrocarbon pool (HP) mechanism that has been well studied for methanol³⁹ is operative for biomass pyrolysis vapors. However, we have not been able to find any information in the literature that discusses phenols as intermediates in this process. Some papers discuss formation of phenols from furan⁵⁸ and acetone.⁵⁹⁻⁶¹
4. Deactivation appears to occur primarily by the build-up of coke on the exterior surface of the catalyst particles that eventually results in a capping of the micropores.

ACKNOWLEDGEMENTS

This work was supported by the U.S. Department of Energy's Bioenergy Technologies Office (DOE-BETO) Contract No. DE-AC36-08GO28308 with the National Renewable Energy Laboratory. Albemarle is acknowledged for providing the catalyst sample. The authors would like to thank, Lynn Gedvilas, Kristen Ryan, John Yarbrough, Sridhar Budhi, Daniel Carpenter, Rick French, and Stefan Czernik for stimulating discussions.

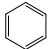
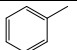
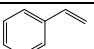
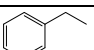
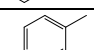
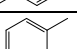
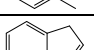
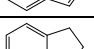
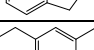
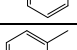
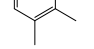
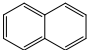
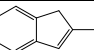
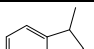
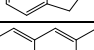
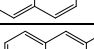
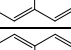
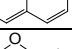
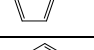
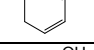
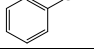
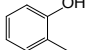
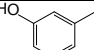
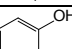
References

1. A. V. Bridgwater, *Fast Pyrolysis of Biomass: A Handbook*, CPL Press, Newbury, UK, 1999.
2. A. V. Bridgwater, *Fast Pyrolysis of Biomass: A Handbook Volume 2*, CPL Press, Newbury, UK, 2002.

3. A. V. Bridgwater, *Fast Pyrolysis of Biomass: A Handbook Volume 3*, CPL Press, Newbury, UK, 2005.
4. A. Oasmaa, E. Leppamaki, P. Koponen, J. Levander and E. Tapola, in *VTT Publications* 1997, vol. 306, pp. 1-87.
5. A. Oasmaa and C. Peacocke, in *VTT Publications* 2001, vol. 450, pp. 1-102.
6. A. Oasmaa and C. Peacocke, in *VTT Publications* 2010, vol. 731, pp. 1-134.
7. R. C. Petterson, in *The Chemistry of Solid Wood (Advances in Chemistry Series)*, ed. R. M. Rowell, American Chemical Society, 1984, pp. 57-126.
8. P. M. Mortensen, J. D. Grunwaldt, P. A. Jensen, K. G. Knudsen and A. D. Jensen, *Appl. Catal., A*, 2011, **407**, 1-19.
9. D. C. Elliott, *Energy Fuels*, 2007, **21**, 1792-1815.
10. J. D. Adjaye and N. N. Bakhshi, *Fuel Process. Technol.*, 1995, **45**, 161-183.
11. J. D. Adjaye and N. N. Bakhshi, *Fuel Process. Technol.*, 1995, **45**, 185-202.
12. F. A. Agblevor, S. Beis, O. Mante and N. Abdoulmoumine, *Ind. Eng. Chem. Res.*, 2010, **49**, 3533-3538.
13. F. A. Agblevor, O. Mante, N. Abdoulmoumine and R. McClung, *Energy Fuels*, 2010, **24**, 4087-4089.
14. E. Antonakou, A. Lappas, M. H. Nilsen, A. Bouzga and M. Stocker, *Fuel*, 2006, **85**, 2202-2212.
15. A. A. Boateng, C. A. Mullen, C. M. McMahan, M. C. Whalen and K. Cornish, *J. Anal. Appl. Pyrolysis*, 2010, **87**, 14-23.
16. T. R. Carlson, T. R. Vispute and G. W. Huber, *Chemsuschem*, 2008, **1**, 397-400.
17. S. Czernik, R. French, A. Stanton and K. Iisa, NREL Milestone Report, 2012, p. 12.
18. J. Diebold and J. Scahill, *ACS Symp. Ser.*, 1988, **376**, 31-40.
19. R. J. Evans and T. A. Milne, *Energy Fuels*, 1987, **1**, 123-137.
20. R. J. Evans and T. A. Milne, in *Pyrolysis Oils from Biomass*, eds. E. J. Soltes and T. A. Milne, ACS Symposium Series, Washington, DC, 1988, ch. 26, pp. 311-327.
21. R. French and S. Czernik, *Fuel Process. Technol.*, 2010, **91**, 25-32.
22. A. G. Gayubo, A. T. Aguayo, A. Atutxa, B. Valle and J. Bilbao, *J. Chem. Technol. Biotechnol.*, 2005, **80**, 1244-1251.
23. A. G. Gayubo, B. Valle, A. T. Aguayo, M. Olazar and J. Bilbao, *Ind. Eng. Chem. Res.*, 2010, **49**, 123-131.
24. T. Q. Hoang, X. Zhu, T. Danuthai, L. L. Lobban, D. E. Resasco and R. G. Mallinson, *Energy Fuels*, 2010, **24**, 3804-3809.
25. P. A. Horne and P. T. Williams, *J. Anal. Appl. Pyrolysis*, 1995, **34**, 65-85.
26. C. A. Mullen, A. A. Boateng, D. J. Mihalcik and N. M. Goldberg, *Energy Fuels*, 2011, **25**, 5444-5451.
27. E. Putun, B. B. Uzun and A. E. Putun, *Energy Fuels*, 2009, **23**, 2248-2258.
28. S. D. Stefanidis, K. G. Kalogiannis, E. F. Iliopoulou, A. A. Lappas and P. A. Pilavachi, *Bioresour. Technol.*, 2011, **102**, 8261-8267.
29. M. J. A. Tijmensen, A. P. C. Faaij, C. N. Hamelinck and M. R. M. van Hardeveld, *Biomass Bioenergy*, 2002, **23**, 129-152.
30. B. Valle, A. G. Gayubo, A. T. Aguayo, M. Olazar and J. Bilbao, *Energy Fuels*, 2010, **24**, 2060-2070.
31. T. P. Vispute, H. Zhang, A. Sanna, R. Xiao and G. W. Huber, *Science*, 2010, **330**, 1222-1227.
32. S. Vitolo, B. Bresci, M. Seggiani and M. G. Gallo, *Fuel*, 2001, **80**, 17-26.
33. S. Vitolo, M. Seggiani, P. Frediani, G. Ambrosini and L. Politi, *Fuel*, 1999, **78**, 1147-1159.
34. P. T. Williams and N. Nugranad, *Energy*, 2000, **25**, 493-513.
35. A. H. Zacher, D. Santosa, D. C. Elliott and C. D. B. Brown, *TCBiomass 2011*, 2011.
36. H. Zhang, R. Xiao, H. Huang and G. Xiao, *Bioresour. Technol.*, 2009, **100**, 1428-1434.
37. D. M. Bibby, R. F. Howe and G. D. McLellan, *Appl. Catal., A*, 1992, **93**, 1-34.
38. D. M. Bibby, N. B. Milestone, J. E. Patterson and L. P. Aldridge, *J. Catal.*, 1986, **97**, 493-502.
39. K. Hemelsoet, J. Van der Mynsbrugge, K. De Wispelaere, M. Waroquier and V. Van Speybroeck, *Chemphyschem*, 2013, **14**, 1526-1545.
40. S. Ilias and A. Bhan, *ACS Catalysis*, 2013, **3**, 18-31.
41. U. Olsbye, S. Svelle, M. Bjorgen, P. Beato, T. V. W. Janssens, F. Joensen, S. Bordiga and K. P. Lillerud, *Angewandte Chemie-International Edition*, 2012, **51**, 5810-5831.
42. J. Diebold and J. Scahill, *ACS Symp. Ser.*, 1988, **376**, 264-276.
43. R. D. Perlack and B. J. Stokes, ed. D.O.E, ORNL/TM-2011/224, Oak Ridge National Laboratory, 2011, pp. 1-227.
44. K. Wang, K. H. Kim and R. C. Brown, *Green Chem.*, 2013.
45. F. Bauer and H. G. Karge, in *Characterization II*, eds. H. Karge and J. Weitkamp, Springer Berlin Heidelberg, 2007, vol. 5, ch. 5, pp. 249-364.
46. M. Guisnet, L. Costa and F. R. Ribeiro, *J. Mol. Catal. A: Chem.*, 2009, **305**, 69-83.
47. M. Guisnet and P. Magnoux, *Appl. Catal., A*, 2001, **212**, 83-96.
48. A. Aho, N. Kumar, K. Eranen, T. Salmi, M. Hupa and D. Y. Murzin, *Fuel*, 2008, **87**, 2493-2501.
49. X. Guo, Y. Zheng and J. Chen, *Biomass Bioenergy*, 2009, **33**, 1469-1473.
50. J. Olstad, J. W., D. Carpenter and D. J. Robichaud, ed. D.O.E, NREL, Golden. CO, 2012, pp. 1-25.

51. R. J. Evans and T. A. Milne, *Energy Fuels*, 1987, **1**, 311-319.
52. M. W. Jarvis, T. J. Haas, B. S. Donohoe, J. W. Daily, K. R. Gaston, W. J. Frederick and M. R. Nimlos, *Energy Fuels*, 2011, **25**, 324-336.
53. E. D. Malinowski, *Factor Analysis in Chemistry*, Wiley, New York, 1991.
54. A. Saito and H. C. Foley, *Microporous Mater.*, 1995, **3**, 543-556.
55. C. Branca, P. Giudicianni and C. Di Blasi, *Ind. Eng. Chem. Res.*, 2003, **42**, 3190-3202.
56. C. Mukarakate, A. M. Scheer, D. J. Robichaud, M. W. Jarvis, D. E. David, G. B. Ellison, M. R. Nimlos and M. F. Davis, *Rev. Sci. Instrum.*, 2011, **82**.
57. A. Corma, *J. Catal.*, 2003, **216**, 298-312.
58. Y.-T. Cheng and G. W. Huber, *ACS Catalysis*, 2011, **1**, 611-628.
59. A. I. Biaglow, J. Sepa, R. J. Gorte and D. White, *J. Catal.*, 1995, **151**, 373-384.
60. A. G. Panov and J. J. Fripiat, *J. Catal.*, 1998, **178**, 188-197.
61. G. S. Salvapati, K. V. Ramanamurty and M. Janardanarao, *J. Mol. Catal.*, 1989, **54**, 9-30.
62. C. A. Querini, in *Catalysis*, eds. J. J. Spivey and G. W. Roberts, The Royal Society of Chemistry, 2004, vol. 17.
63. J. Weitkamp and S. Maixner, *Zeolites*, 1987, **7**, 6-8.
64. Y. T. Chua and P. C. Stair, *J. Catal.*, 2003, **213**, 39-46.
65. J. Li, G. Xiong, Z. Feng, Z. Liu, Q. Xin and C. Li, *Microporous Mesoporous Mater.*, 2000, **39**, 275-280.
66. A. H. Janssen, A. J. Koster and K. P. de Jong, *J. Phys. Chem. B*, 2002, **106**, 11905-11909.
67. K. J. Kim and H. G. Ahn, *Microporous Mesoporous Mater.*, 2012, **152**, 78-83.
68. S. Morin, P. Ayrault, N. S. Gnep and M. Guisnet, *Appl. Catal., A*, 1998, **166**, 281-292.
69. K. Morishige and K. Yoshida, *J. Phys. Chem. B*, 2010, **114**, 7095-7101.
70. M. S. Rana, J. Ancheyta and P. Rayo, *Catal. Today*, 2005, **109**, 24-32.
71. S. Storck, H. Bretinger and W. F. Maier, *Appl. Catal., A*, 1998, **174**, 137-146.

Table 2. Compounds identified by py-GCMS during the four stages of ZSM-5 activity

Retention Time	m/z	Compound Name	Compound Structure	Assignment Confidence Level (%)	Biomass-to-Catalyst ratio for species to appear
3.0	78	Benzene		94	0.1
4.7	92	Toluene		95	0.1
7.8	104	Styrene		96	0.5
7.0	106	Ethyl benzene		91	0.1
7.2	106	p-Xylene		97	0.1
7.8	106	o-Xylene		87	0.1
12.2	116	Indene		95	0.1
11.9	118	Indane		87	0.1
9.9	120	Benzene, 1ethyl-3-methyl		95	0.1
10.8	120	Benzene, 1,2,3-trimethyl-		97	0.1
16	128	Naphthalene		94	0.1
15.1	130	2-Methylindene		90	0.1
14.8	132	Indane, 1-methyl-		93	0.1
18.9	142	Naphthalene, 2-methyl-		91	0.1
21.5	156	Naphthalene, 2,6-dimethyl-		97	0.1
21.5	156	Naphthalene, 2,7-dimethyl-		98	0.2
2.6	82	Furan, 2-methyl		96	0.5
2.9	80	1,3-Cyclohexadiene		92	0.5
10.7	94	Phenol		89	0.8
12.7	108	Phenol, 2-methyl		95	0.6
13.8	108	Phenol, 3-methyl		93	0.6
13.3	108	Phenol, 4-methyl (change structure)		93	1.4
14.0	132	benzofuran, 2-methyl		92	0.6
2.3	70	Furan, 2,5-dihydro		91	1.4

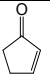
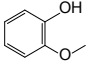
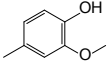
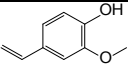
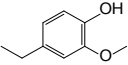
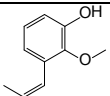
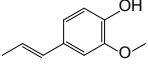
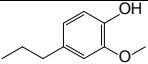
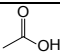
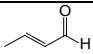
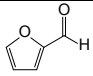
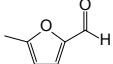
6.4	82	2-Cyclopenten-1-one		93	1.1
13.5	124	Phenol, 2-methoxy		93	1.0
16.3	138	Phenol, 2-methoxy-4-methyl-		96	1.0
19.3	150	2-Methoxy-4-vinylphenol		91	1.1
18.5	152	Phenol, 4-ethyl-2-methoxy-		91	1.1
20.4	164	Phenol, 2-methoxy-3-(2-propenyl)-		98	1.1
22.5	164	Phenol, 2-methoxy-4-(1-propenyl)-		97	1.1
20.6	166	Phenol, 2-methoxy-4-propyl-		68	1.4
2.7	60	Acetic acid		91	1.8
2.9	70	2-Butenal		87	1.8
6.2	96	Furfural		93	1.6
10.0	110	2-Furancarboxaldehyde, 5-methyl-		93	1.5

Table 3. Properties of HZSM-5 catalyst expressed as percentage change relative to the regenerated form.

	Regenerated catalyst	Sample 1	Sample 2	Sample 3	Sample 4
Biomass-to-catalyst ratio	0	0.4	1.0	1.7	5
EDS Atomic Carbon (%)	6.1(5.8)	4.6(3.7)	8.3(6.1)	12.5(4.3)	20.3(5.2)
AFM Surface Roughness (%)	13.77(4.44)	9.52(1.96)	7.46(3.09)	5.83(1.30)	4.92(2.95)
Surface Area m^2/g (BET) (%)	0	12	19	44	67
Pore volume cm^3/g (BJH _{ads}) (%)	0	27	28	43	52
Average pore width Å (BJH _{ads}) ¹ (%)	0	17	6	11	17
Micropore volume ² cm^3/g (%)	0	22	26	48	84
Surface Area m^2/g (t-plot) (%)	0	16	21	48	73
Surface Area m^2/g (t-plot) (%)	0	10	17	38	61
TGA coke (%)	0	6.4	7.8	13.0	15.5
Mesopore carbon (coke)	0	5.9	4.6	8.9	10.8
Micropore carbon	0	0.5	3.2	4.1	4.7

¹Halsey thickness curve, Faas BJH correction.

²High resolution, low pressure adsorption isotherm analysis. (P/P_0 .000001 - .01)

³ Micropore surface area calculated by t-plot

⁴ External surface area calculated by t-plot

